Full-Wave Analysis of Superconducting Microstrip Lines on Anisotropic Substrates Using Equivalent Surface Impedance Approach

Laurence H. Lee, *Student Member, IEEE,* W. Gregory Lyons, *Member, IEEE,* Terry P. Orlando, *Member, IEEE,* Sami M. Ali, *Senior Member, IEEE,* and Richard S. Withers, *Member, IEEE*

Abstract—**A computationally efficient full-wave technique is developed to analyze single and coupled superconducting microstrip lines on anisotropic substrates. The optic axis of the dielectric is in the plane of the substrate at an arbitrary angle with respect to the propagation direction. A dyadic Green's function for layered, anisotropic media is used to formulate an integral equation for the current in the strips. To increase the efficiency of the method, the superconducting strips are replaced by equivalent surface impedances which account for the loss and kinetic inductance of the superconductors. The validity of this equivalent surface impedance (ESI) approach is verified by comparing the calculated complex propagation constant and characteristic impedance for superconducting microstrip lines on an isotropic substrate to measured results, and to numerical results by the more rigorous volume-integral equation method. The results calculated using the ESI approach for perfectly conducting coupled lines on an anisotropic substrate agree with the results by the finite-difference time-domain method. This efficient ESI technique is then used to study the effects of the optic axis orientation and the strip width on the characteristics of single and coupled superconducting microstrip lines on M-plane sapphire. The effects of the line separation and operating temperature on the coupled lines are also investigated.**

I. Introduction

THE performance advantages of superconducting microwave devices have been demonstrated in the form of very high Q planar resonators, long delay lines, and multipole narrowband filters with low insertion loss [1], [2]. The proper choice of substrate materials is a key to the performance of these devices. The uniform and low-loss dielectric properties of sapphire make it attractive for high-temperature superconducting passive microwave device applications. The performance of microwave devices on sapphire has been demonstrated in the form of a broadband, low-loss 9-ns delay line [3] and a 4-pole microstrip filter operating at 10 GHz [4]. However, the anisotropic dielectric property of sapphire requires special attention in the design of these devices. Full-wave methods are essential to achieve the high accuracy required for future high-performance superconducting microwave devices.

Several authors have proposed full-wave analyses of superconducting planar transmission lines on isotropic substrates [5]–[9]. Kessler *et al.* [5] have investigated a coplanar waveguide structure using a mode matching technique. In [6], [7], a spectral-domain volume-integral-equation (SDVIE) method has been proposed to analyze superconducting microstrip lines, striplines, and coplanar waveguides. These two methods rigorously account for the finite volume of the superconductors, yielding accurate characterization for the kinetic inductance and loss. However, both of these methods are computationally inefficient. Pond *et al.* [8] have used a resistive boundary condition to analyze microstrip structures with very thin metalization. A similar method has been used by Nghiem *et al.* [9] to study microstrip lines and striplines for the cases when the superconductor is either much thinner or much thicker than the penetration depth. Both Pond and Nghiem have used the surface impedance derived for a very thin, infinitely extended plate to replace a superconducting strip. Nghiem has also considered the case of using the surface impedance for a very thick, infinitely extended plate to replace a superconducting strip. Because of the different field behaviors in a superconducting strip compared to an infinitely extended plate, the loss and kinetic effect of the superconducting strip are not correctly determined. Pond has pointed out that the singular behavior of the currents at the edges of an infinitely thin strip might increase the kinetic inductance contribution resulting in an enlarged propagation constant.

In this paper, an efficient full-wave method is developed to calculate the effective dielectric constant, attenuation, and characteristic impedance of superconducting microstrip lines and coupled lines on anisotropic substrates. The case of M-plane sapphire is considered in which the optic axis of the substrate is in the plane of the substrate at an arbitrary angle with respect to the propa-

Manuscript received March 30, 1993; revised June 21, 1993. This work was conducted under the auspices of the Consortium for Superconducting Electronics with the full support of the Advanced Research Projects Agency (Contract MDA972-90-C-0021).

L. H. Lee and T. P. Orlando are with the Department of Electrical Engineering and Computer Science and Research Laboratory of Electronics, Massachusetts Institute of Technology, Cambridge, MA 02139.

W. G. Lyons is with Lincoln Laboratory, Massachusetts Institute of Technology, Lexington, MA 02173.

S. M. Ali was with the Department of Electrical Engineering and Computer Science and Research Laboratory of Electronics, Massachusetts Institute of Technology, Cambridge, MA 02139. He is currently with the Ministry of P.T.T., Telecom College, Jeddah, Saudi Arabia.

R. S. Withers is with Conductus, Inc., Sunnyvale, CA 94086.

IEEE Log Number 9212995.

gation direction. To increase the efficiency of the method, the superconducting strips are transformed into infinitely thin strips using an equivalent surface impedance (ESI) concept. These equivalent surface impedances account for the loss and kinetic inductance of the superconductors. A 2-D dyadic Green's function is then used to formulate an integral equation for the surface current in the strips. Galerkin's method with entire-domain basis functions is used to solve for the complex propagation constants. The characteristic impedances are then determined using the power–current definition. To verify the validity of the ESI approach, numerical results for superconducting microstrip lines on isotropic $LaAlO_3$ are compared to previously published measured data and results calculated by the SDVIE method. The effective dielectric constants calculated for perfectly conducting coupled lines on sapphire show good agreement with the results by the finite-difference time-domain method. This efficient ESI technique is then used to study the effects of the optic axis orientation and the strip width on the characteristics of single and coupled superconducting microstrip lines on M-plane sapphire. The effects of the line separation and operating temperature on the coupled lines are also investigated.

By utilizing the ESI concept rather than the more rigorous SDVIE method [6], [7], the computation time is reduced by nearly two orders of magnitude.

II. Method of Solution

In Fig. 1, a superconducting strip is shown on an anisotropic substrate for which the optic axis is in the x-y plane at an angle θ with respect to the y-axis. The thickness of the substrate is assumed to be h. The thickness and the width of the strip are t and $2w$, respectively. The structure is uniform along the propagation direction. A perfectly conducting ground plane is assumed. The permittivity tensor $\bar{\bar{\epsilon}}$ for the substrate in the chosen coordinate system can be written as

$$\bar{\bar{\epsilon}} = \begin{bmatrix} \epsilon_\perp \cos^2\theta + \epsilon_\parallel \sin^2\theta & (\epsilon_\parallel - \epsilon_\perp)\sin\theta\cos\theta & 0 \\ (\epsilon_\parallel - \epsilon_\perp)\sin\theta\cos\theta & \epsilon_\perp \sin^2\theta + \epsilon_\parallel \cos^2\theta & 0 \\ 0 & 0 & \epsilon_\perp \end{bmatrix} \tag{1}$$

where $\epsilon_\perp$ and $\epsilon_\parallel$ are the permittivities perpendicular and parallel to the optic axis, respectively.

A. Equivalent Surface Impedance

To implement an efficient method, an equivalent surface impedance Z_s is used to transform a superconducting strip with a finite thickness into an infinitely thin strip. Since the fields and currents in a superconducting strip behave differently from those in an infinitely extended superconducting plate, the surface impedance derived for an infinite half-plane superconductor or for parallel plates [10] is not suitable for the transformation. Instead, Z_s should preserve the power dissipated and stored in the superconductor. Suppose the thickness of the superconducting strip is on the order of the penetration depth λ or less, then the power associated with the magnetic field can be neglected. The power conservation equation can be simplified to

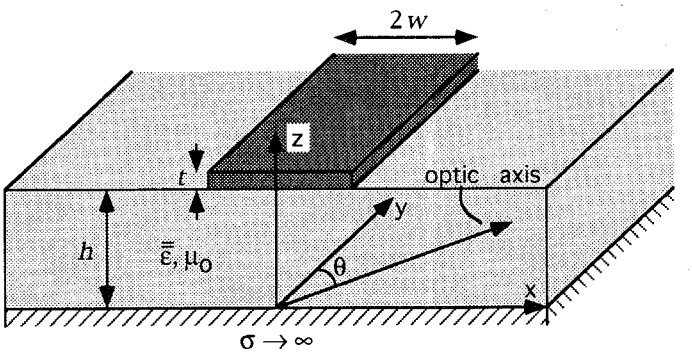

Fig. 1. Superconducting microstrip line with a perfectly conducting ground plane on an anisotropic substrate.

$$\int_{-w}^{w} Z_s |J_{s,y}|^2 \, dx = \frac{1}{\sigma_{sc}} \int_{h}^{h+t} \int_{-w}^{w} |J_y^{(0)}|^2 \, dx \, dz \tag{2}$$

where $J_{s,y}$ is the y-component of the surface current $\bar{J}_s$ in the infinitely thin strip, σ_{sc} is the complex conductivity of the superconductor, and $J_y^{(0)}$ is the y-component of the volume current in the superconducting strip. Both $J_y^{(0)}$ and $J_{s,y}$ are normalized to give a unit current. The simple two-fluid model [11] has been used to describe the complex conductivity σ_{sc} with $\sigma_{sc} = \sigma_1 + i/(\omega\mu_0\lambda^2)$. Throughout the analysis, the exp $(-i\omega t)$ time dependence is used but suppressed.

Because of the edge conditions, the surface current $J_{s,y}$ is infinite at the edges of the strip [12]. The first-order approximation for $J_{s,y}$ can be taken as

$$J_{s,y} \propto \frac{1}{\sqrt{1 - (x/w)^2}}. \tag{3}$$

However, because the y-component of the electric field $(E_y = Z_s J_{s,y})$ is finite at the edges, Z_s should cancel the singularity of $J_{s,y}$ at the edges. Since $E_y \ll E_x$ and E_z for quasi-TEM propagation, we can assume a uniform distribution of E_y across the strip without introducing significant error. Based upon these assumptions, the equivalent surface impedance takes the following form:

$$Z_s(x) = \mathcal{Z}\sqrt{1 - (x/w)^2} \tag{4}$$

where

$$\mathcal{Z} = \frac{w\pi}{\sigma_{sc}} \int_{h}^{h+t} \int_{-w}^{w} |J_y^{(0)}|^2 \, dx \, dz. \tag{5}$$

The volume current $J_y^{(0)}$ remains nearly frequency independent as long as the penetration depth λ is much less than the skin depth δ. When the strip is thin and the substrate is thick, $J_y^{(0)}$ can be well approximated by the current in an isolated thin strip. However, the exact distribution of current cannot be put in a simple analytic form.

An approximate solution is determined to be

$$J_y^{(0)}(x, z) = C_0 \frac{\cosh(x/\lambda)}{\cosh(w/\lambda)} + C_1 \frac{\cosh((2z - t)/2\lambda)}{\cosh(t/2\lambda)} \cdot \left[C_2 \frac{\cosh(x/l_1)}{\cosh(w/l_1)} + \frac{1 - \cosh(x/l_2)/\cosh(w/l_2)}{\sqrt{1 - (x/w)^2}} \right] \quad (6)$$

where

$$C_0 = \frac{C_1 \sqrt{w/\lambda}}{\cosh(t/2\lambda)\sqrt{(2\lambda/t)^2 - 0.083}}$$

$$C_2 = (wt/8\lambda^2)^{3/8}$$

$$l_1 = \sqrt{2\lambda t}$$

$$l_2 = 0.77t + 0.52\lambda^2/t.$$

The derivation of (6) will not be discussed here, but instead will be reported in [13].

B. Integral Equation Formulation and Method of Moments

Figure 1 illustrates the configuration of a superconducting microstrip line. The superconducting strip with finite thickness is transformed into an infinitely thin strip by using the ESI concept, as described in the last section. A 2-D dyadic Green's function $\bar{\bar{\mathcal{G}}}(k_x, k_y)$ for layered, anisotropic media (see Appendix A) is used to formulate an integral equation for the surface current in the strip,

$$Z_s(x)\bar{J}_s(x) = \frac{i\omega\mu_0}{2\pi} \int_{-\infty}^{\infty} dk_x \, \bar{\bar{\mathcal{G}}}(k_x, k_{y0}) \cdot \bar{\mathcal{J}}_s(k_x) e^{ik_x x} \quad (7)$$

where k_{y0} is the complex propagation constant and $\bar{\mathcal{J}}_s(k_x)$ is the Fourier transform of $\bar{J}_s(x)$.

To apply the method of moments, the surface current is expressed in terms of a set of orthogonal basis functions, $\bar{J}_s(x) = \Sigma_{n=0}^{N} [\hat{x}a_n X_n(x) + \hat{y}b_n Y_n(x)]$ where

$$X_n(\xi) = \sin[n\pi(\xi + w)/2w] \quad (8)$$

$$Y_n(\xi) = \frac{\cos[n\pi(\xi + w)/2w]}{\sqrt{1 - (\xi/w)^2}} \quad (9)$$

for $|\xi| \le w$. The Fourier transform of $\bar{J}_s(x)$ is given by $\bar{\mathcal{J}}_s(k_x) = \Sigma_{n=0}^{N} [\hat{x}a_n \mathfrak{X}_n(k_x) + \hat{y}b_n \mathcal{Y}_n(k_x)]$ where

$$\mathfrak{X}_n(k_x) = \left(\frac{n\pi}{2w}\right) \frac{e^{-ik_x w}(-1)^n - e^{ik_x w}}{k_x^2 - (n\pi/2w)^2} \quad (10)$$

$$\mathcal{Y}_n(k_x) = \frac{(-i)^n w\pi}{2} \left[J_o\left(k_x w + \frac{n\pi}{2}\right) + (-1)^n J_0\left(k_x w - \frac{n\pi}{2}\right) \right] \quad (11)$$

and J_0 is the Bessel function of the zeroth order.

By applying Galerkin's method, the integral equation for the surface current is transformed into a set of linear equations for the coefficients of the basis functions,

$$\sum_{n=0}^{N} \begin{bmatrix} K_{mn}^{xx} & K_{mn}^{xy} \\ K_{mn}^{yx} & K_{mn}^{yy} \end{bmatrix} \begin{bmatrix} a_n \\ b_n \end{bmatrix} = 0 \quad (12)$$

for $m = 0, 1, \cdots, N$. The elements of the matrix equation are given by

$$K_{mn}^{pq} = \int_{-\infty}^{\infty} dk_x \mathcal{P}_m(-k_x) \mathcal{G}_{pq}(k_x, k_{y0}) \mathcal{Q}_n(k_x) + \delta_{pq} \frac{i2\pi w}{\omega\mu_0} \mathcal{Z} R_{mn}^p \quad (13)$$

where $p = x, y$; $q = x, y$; $\mathcal{P}_m = \mathfrak{X}_m, \mathcal{Y}_m$; $\mathcal{Q}_n = \mathfrak{X}_n, \mathcal{Y}_n$; $\mathcal{G}_{qp}$ is the pqth element of the $\bar{\bar{\mathcal{G}}}$; δ_{pq} is the Kronecker delta function; $\mathcal{Z}$ is defined in (5); and

$$R_{mn}^x = \begin{cases} \dfrac{\pi}{4} - \dfrac{i^{2m}}{2m} J_1(m\pi), & m = n \\ \dfrac{i^{m-n}}{m-n} J_1\left(\dfrac{(m-n)\pi}{2}\right) - \dfrac{i^{m+n}}{m+n} J_1\left(\dfrac{(m+n)\pi}{2}\right), & m \pm n \text{ are even} \\ 0, & m \pm n \text{ are odd} \end{cases} \quad (14)$$

$$R_{mn}^y = \begin{cases} \dfrac{\pi}{2}\left[i^{m+n} J_0\left(\dfrac{(m+n)\pi}{2}\right) + i^{m-n} J_0\left(\dfrac{(m-n)\pi}{2}\right)\right], & m \pm n \text{ are even} \\ 0, & m \pm n \text{ are odd.} \end{cases} \quad (15)$$

Here J_0 and J_1 are the Bessel functions of the zeroth and first order, respectively.

The complex propagation constant k_{y0} is determined so that the matrix equation has a nontrivial solution. The surface current is then obtained by searching for the eigenvector of the coefficient matrix corresponding to the "zero" eigenvalue. The electric field $\bar{\mathcal{E}}(k_x, z)$ and mag-

netic field $\overline{\mathcal{H}}(k_x, z)$ in the spectral domain are obtained in terms of the surface current. The characteristic impedance Z_c of the line is found by calculating the propagating power,

$$Z_c = \frac{1}{2\pi} \frac{\int_{-\infty}^{\infty} \int_0^{\infty} \hat{y} \cdot (\overline{\mathcal{E}} \times \overline{\mathcal{H}}^*)\, dz\, dk_x}{\left| \int_{-w}^{w} J_{s,y}\, dx \right|^2}. \quad (16)$$

The method of solution for the coupled microstrip lines, shown in Fig. 2, is similar to the one for the single microstrip line. The surface current of the coupled lines is expressed in terms of a set of basis functions,

$$J_{s,x}(x) = \sum_{n=0}^{N} a_n^{(1)} X_n(x - s - w) + a_n^{(2)} X_n(x + s + w) \quad (17)$$

$$J_{s,y}(x) = \sum_{n=0}^{N} b_n^{(1)} Y_n(x - s - w) + b_n^{(2)} Y_n(x + s + w) \quad (18)$$

where $a_n^{(1)}$ and $b_n^{(1)}$ are the expansion coefficients for the microstrip line 1 centered at $x = s + w$, $a_n^{(2)}$ and $b_n^{(2)}$ are the expansion coefficients for the microstrip line 2 centered at $x = -(s + w)$, X_n and Y_n are expressed in (8) and (9), and $2s$ is the separation of the strips. The complex propagation constants for the two fundamental modes, c and π modes, are determined using Galerkin's method. The characteristic impedances, Z_{c1}^c, Z_{c2}^c, Z_{c1}^π, and Z_{c2}^π, of the two lines for the two modes are calculated using the power-current definition

$$Z_{c1}^m = \frac{1}{2\pi} \frac{\int_{-\infty}^{\infty} \int_0^{\infty} \hat{y} \cdot (\overline{\mathcal{E}}_m \times \overline{\mathcal{H}}_m^*)\, dz\, dk_x}{|I_1^m|^2 - R|I_2^m|^2} \quad (19)$$

$$Z_{c2}^m = \frac{1}{2\pi} \frac{\int_{-\infty}^{\infty} \int_0^{\infty} \hat{y} \cdot (\overline{\mathcal{E}}_m \times \overline{\mathcal{H}}_m^*)\, dz\, dk_x}{|I_2^m|^2 - |I_1^m|^2/R} \quad (20)$$

where $\overline{\mathcal{E}}_m$ and $\overline{\mathcal{H}}_m$ are the electric and magnetic fields for the $m = c$, π mode in the spectral domain, I_1^m and I_2^m are the longitudinal current in the lines for the m mode, and $R = I_1^c I_1^\pi / I_2^c I_2^\pi$. For symmetric lines ($R = -1$), (19) and (20) reduce to an equation for the m = even (c mode) and m = odd (π mode) impedances.

III. Numerical Results and Discussion

In the calculations, a low-order (N) series of basis functions is found to be sufficient for the frequency range studied in this work. For a single line on an isotropic substrate, $N = 0$ is sufficient. Converged solutions are obtained by using $N = 2$ for single and coupled lines on anisotropic substrates.

Figure 3 shows good agreement between the calculated

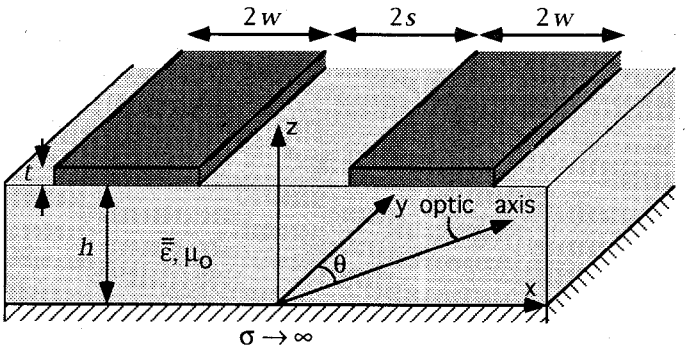

Fig. 2. Superconducting coupled microstrip lines with a perfectly conducting ground plane on an anisotropic substrate.

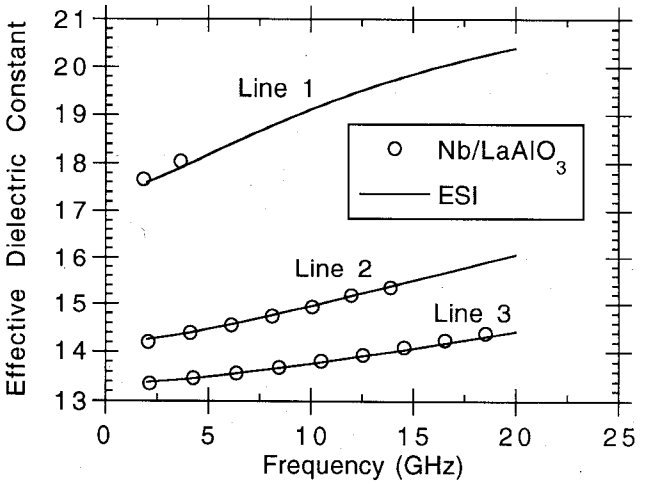

Fig. 3. Measured and calculated effective dielectric constant of three Nb microstrip lines on $LaAlO_3$. The measured results are obtained from [7]. Calculations were performed using the equivalent surface impedance (ESI) approach ($\lambda = 0.0715$ μm; $\sigma_1 = 128$ S/μm; $h = 508$ μm; $t = 0.4$ μm; line 1, $2w = 1800$ μm; line 2, $2w = 181$ μm; and line 3, $2w = 20$ μm).

effective dielectric constants $\epsilon_{\text{eff}} = (\text{Re}\ \{k_{y0}/k_0\})^2$ using the ESI approach discussed here, and the measured data [7] for three Nb microstrip lines on the isotropic substrate $LaAlO_3$ ($\epsilon = 23.5$ and $\tan\delta = 2 \times 10^{-6}$ at 4.2 K). The parameters used for the calculation are those used in [7]. The measured ϵ_{eff} is extracted from the resonant frequency and mode number of the Nb half-wavelength microstrip resonator. Because of the capacitance of the open ends, the resonator is effectively slightly longer than its physical length. The effective length of the resonator is calculated using the expression published in [14].

To demonstrate the necessity of the equivalent surface impedance, Fig. 4 shows the calculated quality factor $Q = \text{Re}\{k_{y0}\}/(2\ \text{Im}\{k_{y0}\})$ of a Nb microstrip line on $LaAlO_3$ as a function of film thickness at 2 GHz. The results by the ESI approach agree well with the results calculated using the SDVIE method [6], [7]. As we have expected, the results calculated using the surface impedance derived for a superconducting parallel-plate to replace the superconducting strip do not agree with the results by ESI or those by SDVIE, except when the strip thickness is thin compared to the penetration depth. The

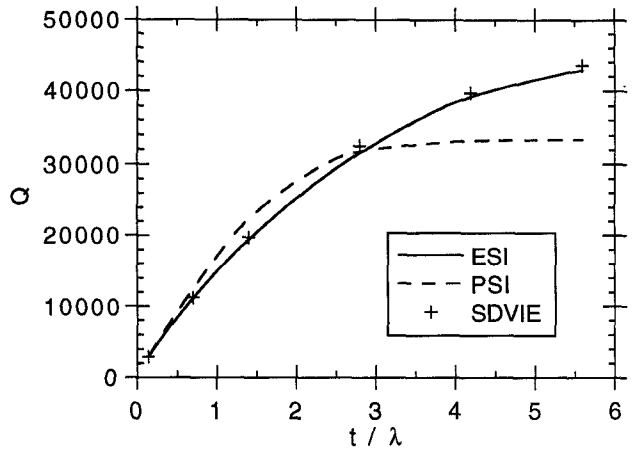

Fig. 4. Calculated quality factor at 2 GHz for a Nb microstrip line on $LaAlO_3$ as a function of strip thickness normalized to the penetration depth. Comparison is made between the ESI approach, the parallel-plate surface impedance (PSI) approach, and the spectral domain volume-integral-equation (SDVIE) method [7] ($\lambda = 0.0715\ \mu m$, $\sigma_1 = 128\ S/\mu m$, $h = 508\ \mu m$, $2w = 20\ \mu m$).

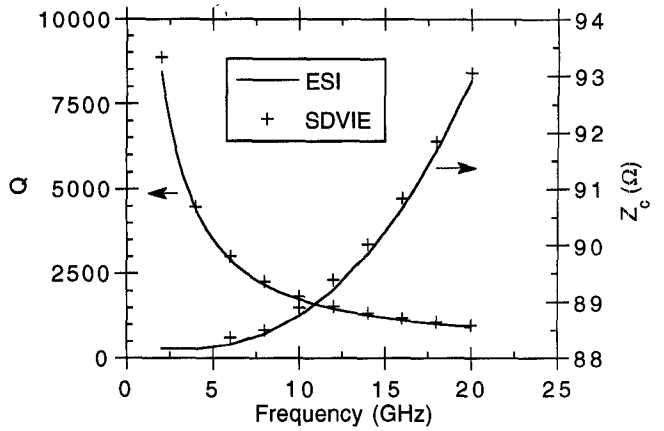

Fig. 5. Calculated quality factor and characteristic impedance of a YBCO microstrip line on $LaAlO_3$ as a function of frequency. Comparison is made between the ESI and the SDVIE approaches [7] ($\lambda = 0.323\ \mu m$, $\sigma_1 = 3.5\ S/\mu m$, $h = 508\ \mu m$, $t = 0.4\ \mu m$, and $2w = 20\ \mu m$).

expression for the superconducting parallel-plate surface impedance used in the calculation can be found in [10],

$$Z_s = \frac{-i\omega\mu_0}{\sqrt{(1/\lambda^2) - i\omega\mu_0\sigma_1}} \coth\left(t\sqrt{(1/\lambda^2) - i\omega\mu_0\sigma_1}\right) \tag{21}$$

which properly accounts for the superconductor in a parallel plate configuration. For a very thin plate $t << \lambda$, (21) approaches $Z_s = 1/(t\sigma_{sc})$. When $t >> \lambda$, (21) approaches the limit for an infinite half-plane, $Z_s = \sqrt{-i\omega\mu_0/\sigma_{sc}}$. To implement the parallel-plate surface impedance (PSI) approach, Galerkin's method cannot be used because the integral equation for the surface current expressed in (7) becomes nonintegrable. Thus, the more general method of moments is applied. However, more basis functions ($N = 8$) are required for the PSI method to obtain convergence than for the ESI method.

In Fig. 5, the quality factor Q and the characteristic impedance Z_c of a YBCO microstrip line, calculated using the ESI approach, are shown together with the numerical results obtained using the SDVIE method. The comparison again shows good agreement, thereby validating the ESI technique. The ESI approach achieves a great saving in the computation time, requiring nearly two orders of magnitude less time than the SDVIE method.

This efficient full-wave method using the ESI approach is then applied to study YBCO microstrip lines ($t = 0.4\ \mu m$) on 430-μm-thick M-plane sapphire substrates ($\epsilon_\perp = 9.34$ and $\epsilon_\parallel = 11.6$). Typical values of $\lambda_0 = 0.22\ \mu m$, $\sigma_1(T_c) = 6.56\ S/\mu m$, and the superconducting transition temperature $T_c = 90$ K for YBCO are used, where λ_0 is the penetration depth at $T = 0$ K, and σ_1 is the real part of σ_{sc}. The operating temperature is assumed to be 77 K. The calculated effective dielectric constant ϵ_{eff}, attenuation constant α, and characteristic impedance Z_c at 2 and 20 GHz for various $2w/h$ ratios are illustrated as functions of θ in Figs. 6–8. Because of the larger dielectric

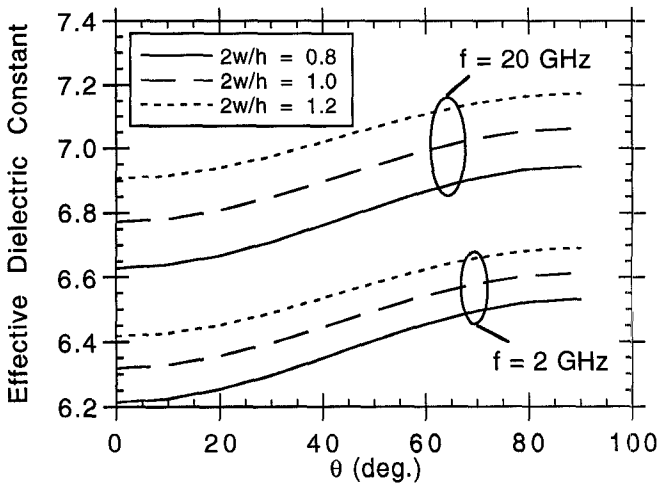

Fig. 6. Calculated effective dielectric constant at 2 and 20 GHz for YBCO microstrip lines on M-plane sapphire as a function of the rotation angle θ of the optic axis. The normalized strip width is used as a parameter ($\lambda = 0.323\ \mu m$, $\sigma_1 = 3.5\ S/\mu m$, $h = 430\ \mu m$, and $t = 0.4\ \mu m$).

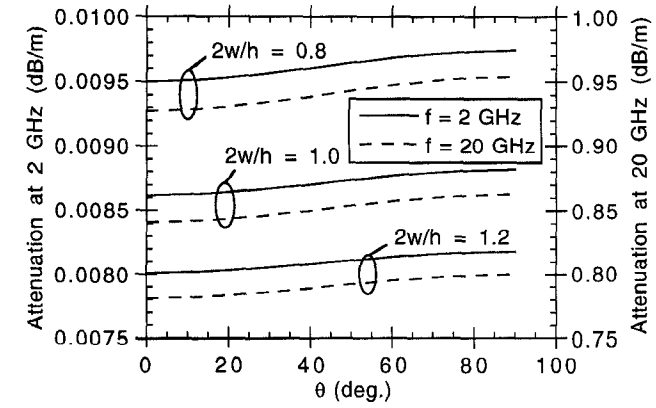

Fig. 7. Calculated attenuation constant at 2 and 20 GHz for YBCO microstrip lines on M-plane sapphire as a function of the rotation angle θ of the optic axis. The normalized strip width is used as a parameter ($\lambda = 0.323\ \mu m$, $\sigma_1 = 3.5\ S/\mu m$, $h = 430\ \mu m$, and $t = 0.4\ \mu m$).

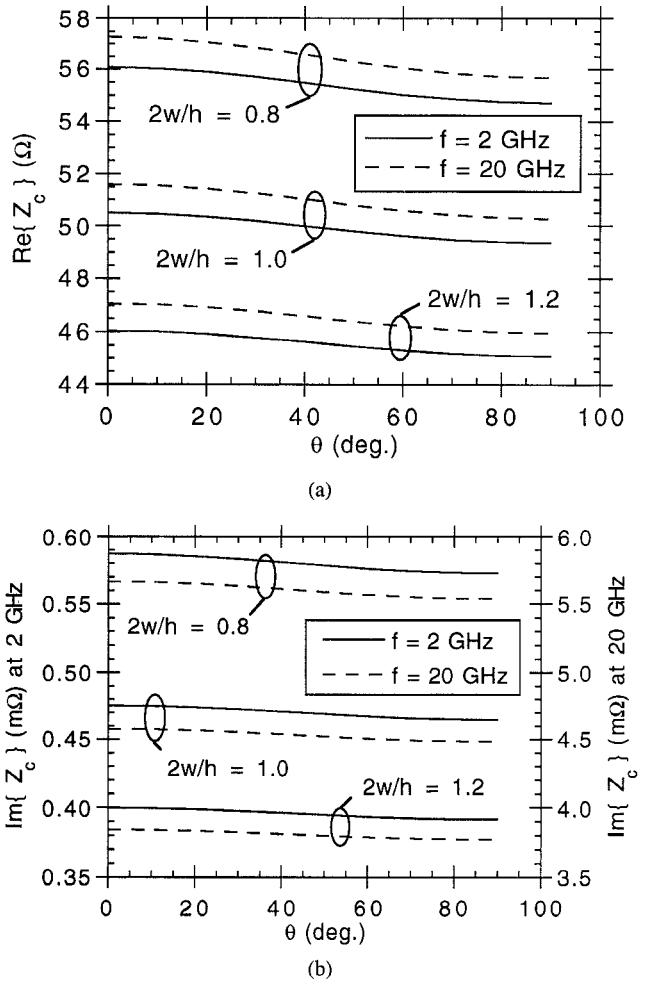

Fig. 8. Calculated (a) real and (b) imaginary parts of the characteristic impedance at 2 and 20 GHz for YBCO microstrip lines on M-plane sapphire as a function of the rotation angle θ of the optic axis. The normalized strip width is used as a parameter ($\lambda = 0.323$ μm, $\sigma_1 = 3.5$ S/μm, $h = 430$ μm, and $t = 0.4$ μm).

constant along the optic axis and the fact that the transverse electric field is much larger than the longitudinal field E_y, the inductance L and capacitance C of the lines increase as θ increases from 0° to 90°. The effective dielectric constant, which is a function of the product of L and C, shows a greater dependence on θ compared to the attenuation constant and the characteristic impedance, which depend on the ratio of L and C. Since the capacitance increases more rapidly with θ than the inductance, the α increases with θ while the Z_c decreases. The rotation of the optic axis about the z-axis changes the effective dielectric constant "seen" by the x-component of the fringing electric field. As the signal strip becomes narrower, the fringing field becomes more significant. Consequently, the effects of the rotation of the optic axis on the characteristics of the lines are greater for smaller $2w/h$. The ϵ_{eff}, α, and Z_c become less dependent on θ as the frequency increases from 2 to 20 GHz. This occurs because the fields for microstrip lines are more confined under the signal strips at higher frequencies.

For symmetric coupled lines, the fundamental modes are called even mode where the longitudinal currents in the lines are in the same direction, and odd mode where the currents are in the opposite direction. In the case of coupled symmetric lines on anisotropic substrates, the field symmetry of the coupled lines no longer exists when the optic axis is not aligned with one of the coordinate axes (i.e., the permittivity tensor has off-diagonal elements). The fundamental modes for coupled lines on anisotropic substrate are generally labeled c and π corresponding to the typical lack of perfect field symmetry. In principle, the impedances of the two coupled microstrip lines are different because of the distortion in the field symmetry. However, in the case of M-plane sapphire the optic axis is in the plane of the substrate. Since the longitudinal component of the electric field is much smaller than the other components, the field symmetry is only slightly distorted when the optic axis is rotated about the z-axis. As a result, the difference in the impedances for the two lines (line 1 and line 2) on M-plane sapphire is negligible. The distortion of field symmetry is much greater in the case where the optic axis of the substrate is in the plane normal to the propagation direction. Although this case is not studied here, the ESI approach can analyze such a structure using the appropriate Green's function.

Figure 9 shows the effective dielectric constant for perfectly conducting coupled microstrip lines on M-plane sapphire. The results calculated using the ESI method compare well with those generated by the finite-difference time-domain method [15]. In applying the ESI method, the equivalent surface impedance Z_s is set to zero for the perfectly conducting strips. The effect of the rotation of the optic axis on the characteristics of YBCO coupled microstrip lines on M-plane sapphire are then studied using the ESI method. The parameters for YBCO and sapphire used in the calculations are those used for the single microstrip lines. The calculated ϵ_{eff}, α, and $\text{Re}\{Z_c\}$ at 2 GHz for the two fundamental modes are illustrated in Figs. 10–12. The results show that the effects of the orientation of the optic axis on the characteristics of coupled lines are similar to the effects on the single lines.

Figures 13–15 show the variation of c- and π-mode ϵ_{eff}, α, and $\text{Re}\{Z_c\}$ with strip width $2w/h$ and separation $2s/h$ for superconducting YBCO coupled microstrip lines on M-plane sapphire at 77 K. The optic axis of the sapphire is again assumed to be aligned with the propagation direction. The characteristics of the π mode behave similarly to coplanar strips. The ϵ_{eff} and $\text{Re}\{Z_c\}$ for the π mode increase with the separation, while the α decreases because of the more uniform current distribution as the separation increases. For the c mode, the calculated results approach the values for two single lines as the separation increases. When the strips are close to each other, the characteristics for the c mode show interesting coupling effects. The interaction of the fields causes the current at the inner edges to peak less, which slightly reduces the attenuation as shown in Fig. 14. As the separation of the lines becomes small, the pattern of the electric and mag-

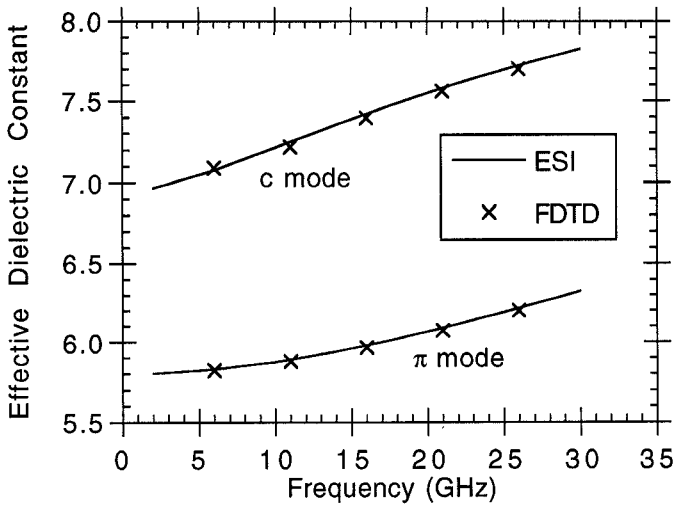

Fig. 9. Effective dielectric constant of a perfectly conducting coupled microstrip line on M-plane sapphire. Comparison is made between the ESI approach and the finite difference time domain (FDTD) method [15] (θ = 45°, $2s/h$ = 1, $2w/h$ = 1, and h = 430 μm).

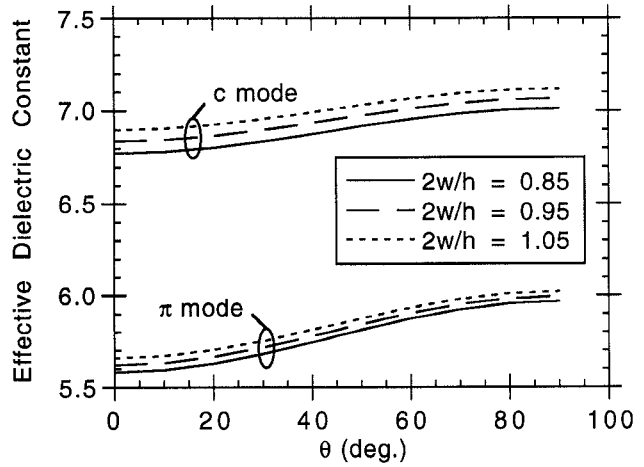

Fig. 10. Calculated c- and π-mode effective dielectric constants of YBCO coupled microstrip lines on M-plane sapphire as functions of the rotation angle θ of the optic axis at 2 GHz (λ = 0.323 μm, σ_1 = 3.5 S/μm, h = 430 μm, $2s/h$ = 1, and t = 0.4 μm).

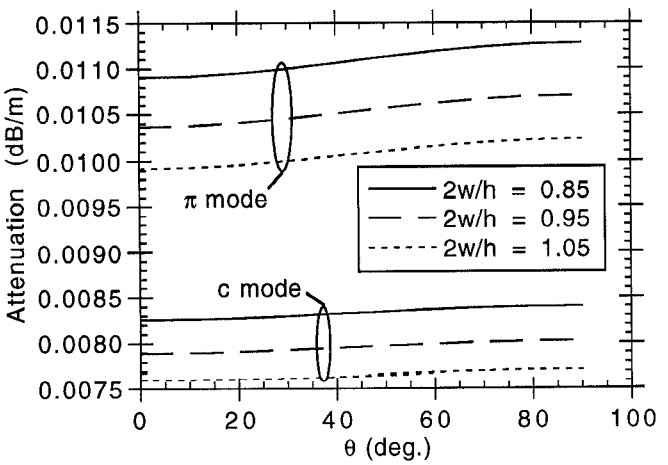

Fig. 11. Calculated c- and π-mode attenuation constants of YBCO coupled microstrip lines on M-plane sapphire as functions of the rotation angle θ of the optic axis at 2 GHz (λ = 0.323 μm, σ_1 = 3.5 S/μm, h = 430 μm, $2s/h$ = 1, and t = 0.4 μm).

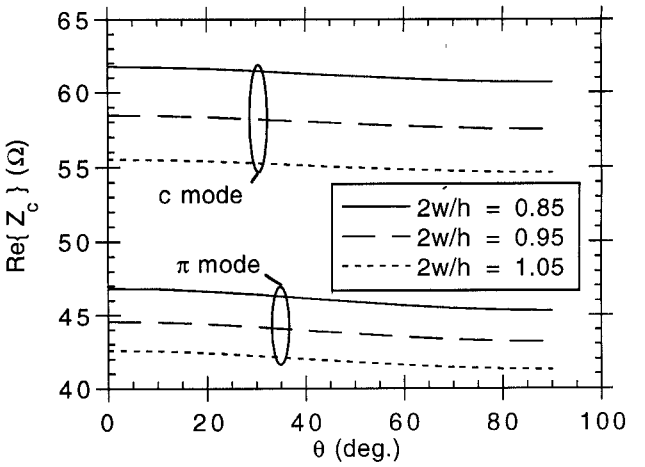

Fig. 12. Calculated c- and π-mode characteristic impedances (real part) of YBCO coupled microstrip lines on M-plane sapphire as functions of the rotation angle θ of the optic axis at 2 GHz (λ = 0.323 μm, σ_1 = 3.5 S/μm, h = 430 μm, $2s/h$ = 1, and t = 0.4 μm).

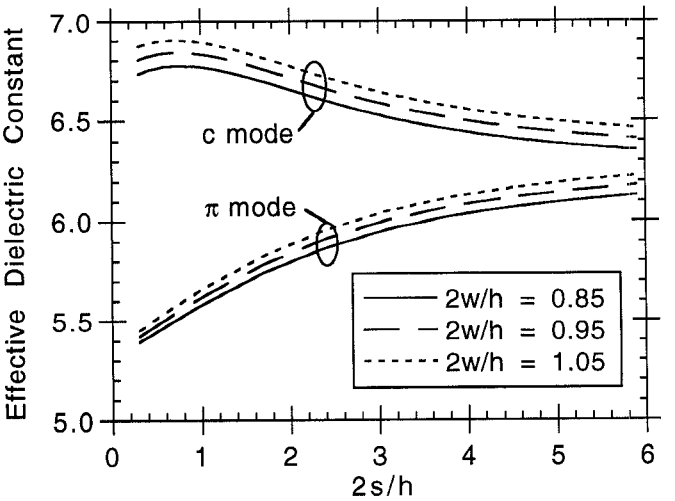

Fig. 13. Calculated c- and π-mode effective dielectric constants of YBCO coupled microstrip lines on M-plane sapphire as functions of the normalized line separation at 2 GHz (λ = 0.323 μm, σ_1 = 3.5 S/μm, h = 430 μm, t = 0.4 μm, and θ = 0°).

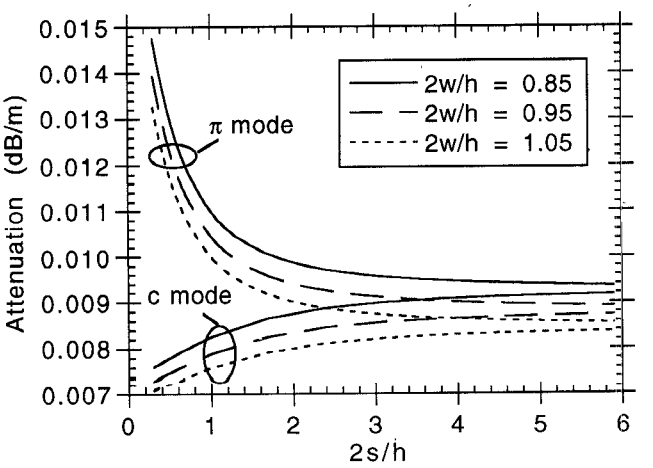

Fig. 14. Calculated c- and π-mode attenuation constants of YBCO coupled microstrip lines on M-plane sapphire as functions of the normalized line separation at 2 GHz (λ = 0.323 μm, σ_1 = 3.5 S/μm, h = 430 μm, t = 0.4 μm, and θ = 0°).

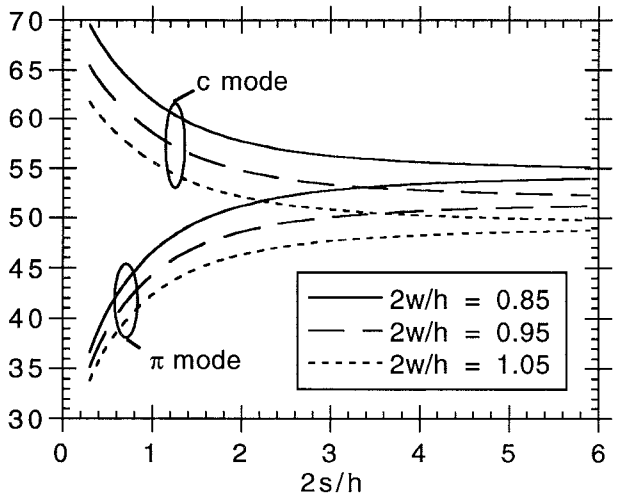

Fig. 15. Calculated c- and π-mode characteristic impedances of YBCO coupled microstrip lines on M-plane sapphire as functions of the normalized line separation at 2 GHz ($\lambda = 0.323$ μm, $\sigma_1 = 3.5$ S/μm, $h = 430$ μm, $t = 0.4$ μm, and $\theta = 0°$).

netic fields approaches the pattern for a single line, and the fringing fields between the strips are reduced. Consequently, the ϵ_{eff} and Re $\{Z_c\}$, shown in Figs. 13 and 15, are larger for smaller $2s/h$. As shown in Fig. 13, when the enhancement of the fringing fields at the outer edges becomes greater than the reduction of the fringing fields at the inner edges, the ϵ_{eff} of the coupled line starts to decrease as the separation is further reduced.

The reliability of superconducting microwave devices depends on their sensitivity to temperature fluctuation. Fig. 16 shows the effects of temperature on the c- and π-mode impedances of YBCO coupled microstrip lines on M-plane sapphire. In the calculations, the simple two-fluid model is used to describe the temperature dependences of the penetration depth, $\lambda(T) = \lambda_0/\sqrt{1 - (T/T_c)^4}$, and the real part of σ_{sc}, $\sigma_1(T) = \sigma_1(T_c)\,(T/T_c)^4$. By assuming the critical temperature T_c is 90 K, operating at 77 K gives $T/T_c = 0.86$. The impedances of the lines are very sensitive to temperature fluctuation as shown in Fig. 16. As we have quantified in our calculations, decreasing the operating temperature from 77 to 60 K would dramatically reduce the sensitivity of the YBCO devices to temperature fluctuation. Furthermore, increasing the thickness of the strips would also reduce the temperature dependence because the kinetic effect of superconductors becomes less for thicker strips.

IV. Conclusions

A computationally efficient full-wave method utilizing the ESI concept is developed for characterization of single and coupled superconducting microstrip lines on anisotropic substrates. The case of M-plane sapphire is considered in which the optic axis of the substrate is in the plane of the substrate at an arbitrary angle with respect to the propagation direction. The calculated results for microstrip lines on isotropic $LaAlO_3$ show good agreement with previously published measured data and with the more

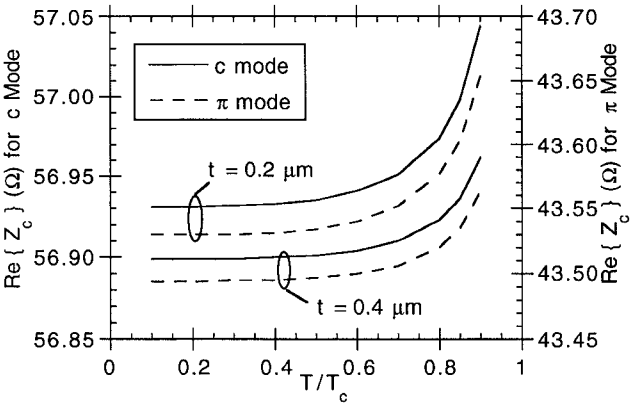

Fig. 16. Calculated c- and π-mode characteristic impedances of YBCO coupled microstrip lines on M-plane sapphire as functions of reduced temperature T/T_c at 2 GHz ($\lambda_0 = 0.22$ μm, $\sigma_1(T_c) = 6.56$ S/μm, $T_c = 90$ K, $2s/h = 1$, $2w/h = 1$, $h = 430$ μm, and $\theta = 0°$).

rigorous volume-integral-equation method. The calculated c- and π-mode effective dielectric constants for perfectly conducting coupled lines on M-plane sapphire compare well with the results generated by the finite-difference time-domain method. The effects of the rotated optic axis of M-plane sapphire on the characteristics of superconducting microstrip lines and coupled lines are presented for various strip widths. The effects of the line separation and operating temperature on the coupled lines are also reported.

V. Acknowledgment

The authors would like to thank C. W. Lam of MIT for providing the finite-difference time-domain results.

Appendix A
Dyadic Green's Function

The dyadic Green's function $\overline{\overline{G}}(k_x, k_y)$ is derived using the method proposed in [16]. Let k_0 be the k-vector in the free space. Define $k_\rho^2 = k_x^2 + k_y^2$, $K_0^2 = k_\rho^2 - k_0^2$ and $K_1^2 = k_\rho^2 - \epsilon_\perp k_0^2$. The explicit form of $\overline{\overline{G}}(k_x, k_y)$ is given by

$$\overline{\overline{G}}(k_x, k_y) = \left[\overline{\overline{Q}}^{-1} \cdot \begin{pmatrix} f_1 & 0 \\ 0 & f_2 \end{pmatrix} \cdot \overline{\overline{Q}} + k_0^2\,\Gamma\,\overline{\overline{\epsilon}}_\rho\right]^{-1} \tag{A1}$$

where

$$\overline{\overline{\epsilon}}_\rho = \begin{bmatrix} \epsilon_\perp \cos^2\theta + \epsilon_\parallel \sin^2\theta & (\epsilon_\parallel - \epsilon_\perp)\sin\theta\cos\theta \\ (\epsilon_\parallel - \epsilon_\perp)\sin\theta\cos\theta & \epsilon_\perp \sin^2\theta + \epsilon_\parallel \cos^2\theta \end{bmatrix}$$

$$\overline{\overline{Q}} = \frac{1}{k_\rho}\begin{pmatrix} k_x & k_y \\ -k_y & k_x \end{pmatrix}$$

$$f_1 = -k_0^2\left(\frac{1}{K_0} + \frac{\epsilon_\perp}{K_1^2}\,\Phi\right)$$

$$f_2 = K_0 - k_\rho^2\Gamma + \Phi$$

$$\Gamma = \frac{1}{\lambda_1^2 - \lambda_2^2}\left[\lambda_2 \coth(\lambda_2 h) - \lambda_1 \coth(\lambda_1 h)\right]$$

$$\Phi = \frac{\lambda_1 \lambda_2}{\lambda_1^2 - \lambda_2^2}\left[\lambda_1 \coth(\lambda_2 h) - \lambda_2 \coth(\lambda_1 h)\right]$$

and λ_1^2 and λ_2^2 are the eigenvalues of

$$\bar{\bar{B}} = \begin{pmatrix} \frac{K_1^2}{\epsilon_\perp} & 0 \\ 0 & -k_0^2 \end{pmatrix} \cdot \left[\frac{k_\rho^2}{k_0^2} \begin{pmatrix} 0 & 0 \\ 0 & -1 \end{pmatrix} + \bar{\bar{Q}} \cdot \bar{\bar{\epsilon}}_\rho \cdot \bar{\bar{Q}}^{-1} \right]. \tag{A2}$$

REFERENCES

[1] W. G. Lyons and R. S. Withers, "Passive microwave device applications of high-T_c superconducting thin films," *Microwave J.*, vol. 33, pp. 85–102, Nov. 1990.

[2] R. S. Withers and R. W. Ralston, "Superconductive analog signal processing devices," *Proc. IEEE*, vol. 77, pp. 1247–1263, Aug. 1989.

[3] G.-C. Liang, R. S. Withers, B. F. Cole, and N. Newman, "High-temperature superconducting devices on sapphire," presented at IEEE MTT-S Int. Microwave Symp., Albuquerque, June 1992.

[4] G.-C. Liang, R. S. Withers, B. F. Cole, S. M. Garrison, M. E. Johansson, W. Ruby, and W. G. Lyons, "High-temperature superconducting delay lines and filters on sapphire and thinned $LaAlO_3$ substrates," *IEEE Trans. Appl. Superconduct.*, vol. 3, pp. 3037–3042, Sept. 1993.

[5] J. Kessler, R. Dill, and P. Russer, "Field theory investigation of high-T_c superconducting coplanar waveguide transmission lines and resonators," *IEEE Trans. Microwave Theory Tech.*, vol. 39, pp. 1566–1574, Sept. 1991.

[6] L. H. Lee, S. M. Ali, and W. G. Lyons, "Full-wave characterization of high-T_c superconducting transmission lines," *IEEE Trans. Appl. Superconduct.*, vol. 2, pp. 49–57, June 1992.

[7] L. H. Lee, S. M. Ali, W. G. Lyons, D. E. Oates, and J. D. Goettee, "Analysis of superconducting transmission line structures for passive microwave device applications," *IEEE Trans. Appl. Superconduct.*, vol. 3, pp. 2782–2787, Mar. 1993.

[8] J. M. Pond, C. M. Krowne, and W. L. Carter, "On the application of complex resistive boundary conditions to model transmission lines consisting of very thin superconductors," *IEEE Trans. Microwave Theory Tech.*, vol. 37, pp. 181–190, Jan. 1989.

[9] D. Nghiem, J. T. Williams, and D. R. Jackson, "A general analysis of propagation along multiple-layer superconducting stripline and microstrip transmission lines," *IEEE Trans. Microwave Theory Tech.*, vol. 39, pp. 1553–1565, Sept. 1991.

[10] R. E. Matick, *Transmission Lines for Digital and Communication Networks*. New York: McGraw-Hill, 1969.

[11] T. P. Orlando and K. A. Delin, *Foundations of Applied Superconductivity*. Reading, MA: Addison-Wesley, 1991.

[12] J. Meixner, "The behavior of electromagnetic fields at edges," *IEEE Trans. Antennas Propagat.*, vol. AP-20, pp. 442–446, July 1972.

[13] L. H. Lee, T. P. Orlando, and W. G. Lyons, "Current distribution in superconducting thin-film strips," submitted to *IEEE Trans. Appl. Superconduct.*

[14] K. C. Gupta, R. Garg, and I. J. Bahl, *Microstrip Lines and Slotlines*. Norwood, MA: Artech House, 1979.

[15] C.-W. Lam, S. M. Ali, and T. P. Orlando, "Full-wave analysis of microstrip lines on anisotropic substrates using the finite-difference time-domain method," submitted to *IEEE Trans. Microwave Theory Tech.*

[16] R. Marques and M. Horno, "Dyadic Green's function for microstrip-like transmission lines on a large class of anisotropic substrates," *IEE Proc. H*, vol. 133, pp. 450–454, Dec. 1986.

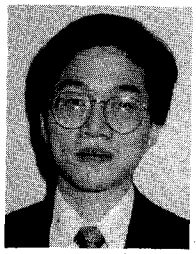

Laurence H. Lee (S'90) received the B.S. degree *summa cum laude* in electrical engineering from the State University of New York, Buffalo, in 1989, and the S.M. degree in electrical engineering from the Massachusetts Institute of Technology, Cambridge, in 1990. He is currently working toward the Ph.D. degree in the Department of Electrical Engineering and Computer Science at MIT.

His research interests are in the areas of microwave integrated circuits, numerical methods for electromagnetic wave problems, and applied superconductivity.

Mr. Lee is a member of Tau Beta Pi.

W. Gregory Lyons (S'81–M'82) received the B.S. (1982), M.S. (1983), and Ph.D. (1989) degrees in electrical engineering from the University of Illinois, Urbana.

Since 1989 he has been a Staff Member in the Analog Device Technology Group at Lincoln Laboratory, Massachusetts Institute of Technology. His graduate work involved the development of microwave and optoelectronic devices based on GaAs and related III-V semiconductor compounds, and the study of collective quantum-mechanical effects in low-dimensional metallic conductors. His recent work includes the development of superconducting microwave devices and the high-performance, high-frequency signal-processing systems that can be built using these devices. This work has been focused mainly on high-temperature superconducting materials.

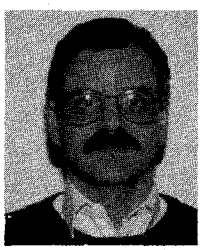

Terry P. Orlando (M'81) received the B.S. degree in physics *summa cum laude* from Louisiana State University in 1974, and the M.S. and Ph.D. in physics from Stanford University in 1976 and 1981, respectively.

Since 1981 he has been at the Massachusetts Institute of Technology where he is a Professor in the Department of Electrical Engineering and Computer Science. His research interests include superconductivity and quantum-effect semiconducting devices. He has also coauthored the textbook, *Foundations of Applied Superconductivity*, and is presently Program Chairman for the 1994 Applied Superconductivity Conference.

Sami M. Ali (M'79–SM'86) received the Ph.D. degree in electrical engineering from the Technical University of Prague, Czechoslovakia, in 1975.

From 1965 to 1985, he was with the Electrical Engineering Department, Military Technical College, Cairo, Egypt. From 1981 to 1982, he spent a sabbatical leave as a visiting scientist at the Massachusetts Institute of Technology, Cambridge. In 1985 he became a Professor and Head of the Basic Electrical Engineering Department at the Military Technical College. From 1987 to 1989, he was a visiting scientist at the Massachusetts Institute of Technology where he joined the Research Staff in 1989. In 1993, he joined the Telecom College, Jeddah, Saudi Arabia. His current research interests deal with microwave integrated circuits, microstrip antennas, and modeling of superconducting microwave devices.

Richard S. Withers, for a photograph and biography, see this issue, p. 2375.